Frequency-Selective Surfaces to Enhance Performance of Broad-Band Reconfigurable Arrays

Yunus E. Erdemli, *Member, IEEE*, Kubilay Sertel, Roland A. Gilbert, *Member, IEEE*, Daniel E. Wright, and John L. Volakis, *Fellow, IEEE*

***Abstract*—In this paper, we present a novel frequency-selective surface (FSS) design aimed at enhancing the performance of broad-band reconfigurable antenna apertures. In particular, reconfigurable printed dipole arrays are examined in the presence of a multilayer FSS. Of particular interest is the design of FSS structures whose reflection coefficient has prespecified phase response over a broad set of frequencies. Previous FSSs primarily considered designs on the basis of the reflection-coefficient amplitude and were intended for radome applications rather than substrates. Designing FSSs subject to phase requirements will be seen to require some compromise in the magnitude. Broad-band requirements also present us with a need for noncommensurate FSS designs.**

***Index Terms*—Broad-band substrate design, hybrid finite-element boundary-integral method, multilayer frequency-selective surfaces, noncommensurate structures, reconfigurable antenna apertures.**

I. Introduction

CONFORMAL antennas are often printed on a planar or curved substrate surface. However, typical substrate configurations are narrowband, and thicker substrates result in low efficiencies due to surface wave coupling. Perforated or bandgap substrates have recently been used to increase the efficiency of printed antennas on thicker substrates [1], [2]. However, these approaches are still applicable only to narrowband or multiband antenna structures. When traditional broad-band antennas such as log-periodics are printed on substrates, their bandwidth characteristics are altered, and one approach to regain the broad-band behavior of the antenna element is to employ frequency-dependent substrates or ground planes (GPs). This can be achieved by using multiple layers of frequency selective surfaces (FSSs) [3] as part of the substrate in a manner similar to that used for designing broad-band microwave filters. Each screen is resonant at a given frequency and is placed a distance $\lambda_s/4$ away from the antenna's surface, where λ_s refers to the wavelength at the screen's resonance frequency.

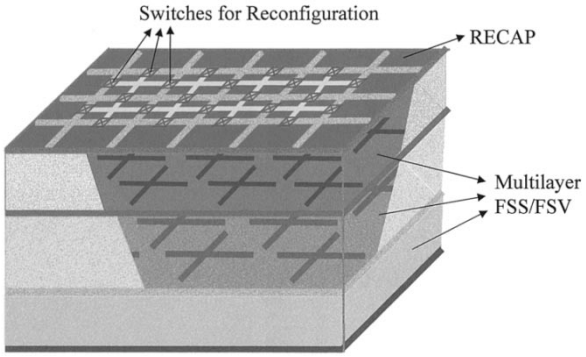

Fig. 1. Reconfigurable antenna aperture (RECAP) over a multilayer FSS/FSV structure.

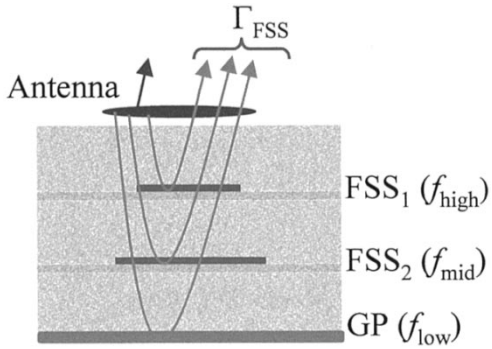

Fig. 2. Coherence between antenna radiation and reflections from the substrate provides broad-band operation.

A multilayer FSS or frequency-selective volume (FSV) configuration [4]–[6] is needed for optimizing the performance of a broad-band antenna. Such a structure is illustrated in Fig. 1. In this paper, we examine various designs of such volumetric periodic surfaces that can be used to enhance the performance of reconfigurable broad-band antenna arrays (see Fig. 1). Of particular interest is the development of such multilayer FSSs, which reflect with prespecified phase and amplitude of the reflection coefficient over a broad set of frequencies. When the phase is actually maintained near zero degrees, such FSSs serve to emulate magnetic GPs. As such, they can substantially enhance the radiation properties of printed antennas placed over the FSS since the reflected field will be in phase with that directly radiated by the antenna itself (see Fig. 2). When the FSS is designed to deliver nearly constant phase over a broad bandwidth, substantial

Manuscript received November 10, 2000; revised May 31, 2001. This work was supported by DARPA/RECAP Program.

Y. E. Erdemli, was with the Radiation Laboratory, Electrical Engineering and Computer Science Department, University of Michigan, Ann Arbor, MI 48109-2122 USA. He is now with the Department of Electronics and Computer Education, Kocaeli University, 41050 Ismit, Turkey.

K. Sertel is with the Radiation Laboratory, Electrical Engineering and Computer Science Department, University of Michigan, Ann Arbor, MI 48109-2122 USA.

R. A. Gilbert and D. E. Wright are with BAE Systems, Nashua, NH 03060-0868 USA.

J. L. Volakis is with The Ohio State University, Columbus, OH 43210 USA.

Digital Object Identifier 10.1109/TAP.2002.807377

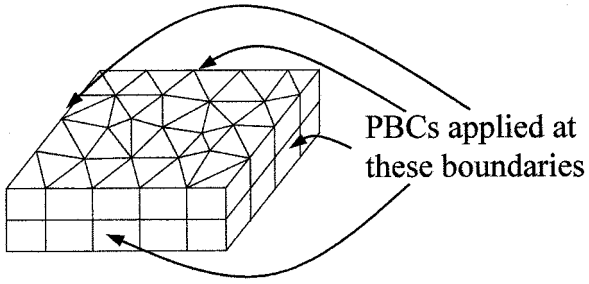

Fig. 3. Prismatic FE mesh for a commensurate unit cell.

gain enhancement can be achieved over a wide range of frequencies. In the past, FSS designs were mostly concerned with amplitude responses. For FSS GPs, the emphasis is on phase. One way to achieve smooth phase responses is to compromise the amplitude response and in this paper, we demonstrate this effect. In addition, using full-wave finite element-boundary integral (FE-BI) simulations, we demonstrate the bandwidth improvements achieved for a dipole array on such an FSS. Reconfiguration of the dipole is also considered in our study. In this case, the dipole length is altered (using diode or MEMS switches) to operate at a different band without a need for changing the FSS design that serves as a "substrate." Broad bandwidth requirements also present us with a need for noncommensurate FSS designs. Hence, modeling of multilayer FSSs with different periodicities [7] is another important issue that will be addressed in the paper.

II. Full-Wave Analysis

The hybrid FE-BI method [8] is used for the analysis of multilayer FSS structures of interest. An important aspect of this hybrid technique is the ability to simulate and design structures that are complex in geometry and incorporate a variety of materials. A multilayer FSS or a FSV in the presence of an antenna array is one such structure (Fig. 1). As is often the case, the highly adaptable FE method is used for modeling the multilayer dielectric region of the array, whereas the BI serves as a means of truncating the finite-element mesh. The BI submatrix typically consumes most of the CPU requirements. Therefore, a recently introduced scheme referred to as the fast spectral-domain algorithm (FSDA) is employed to speed up the BI calculations in the context of iterative solvers [9]. As compared to the adaptive-integral method (AIM), the FSDA often provides two orders of magnitude faster solutions with memory as well as CPU complexity of $O(N)$. Thus, the adaptability of the FE-BI method along with the speed-up advantage of the FSDA serves as a very efficient analysis tool while designing antenna arrays with multilayer FSSs.

To model the infinite array problem, the field periodicity condition is enforced at the vertical boundaries of the unit cell [10], [11] (see Fig. 3). Also on the very top (or bottom) surface, the periodic Green's function (PGF) is applied to truncate the aperture. As such, even though the structure is multilayered, by virtue of the FEM, only the free-space PGF is needed, thus simplifying the implementation and reducing computational requirements [12]. A situation of interest is the case of noncommensurate FSS or antenna array structures as

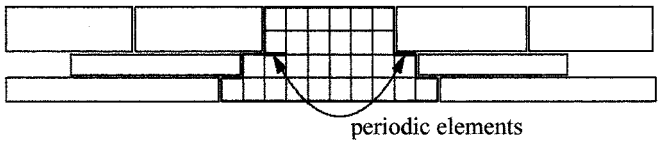

Fig. 4. Decoupling of individual layer periodicities for noncommensurate structures.

shown in Fig. 4. For such situations, the periodic (or phase) boundary conditions (PBCs) cannot be rigorously applied for edges that border two consecutive layers with different periodicities (unless a boundary integral is used at each layer interface). Instead, we choose to use the PBC for the layer just below the edges. Of course, this is only an approximate model as compared to the rigorous approach given in [13], but its accuracy can arbitrarily be improved by grouping several cells in the individual layers.

For validation purposes, a 7×7 finite array of a double-layer Jerusalem cross FSS was first built and reflection coefficient measurements were carried out. The corresponding unit-cell geometry of the noncommensurate structure is shown in Fig. 5 along with the dimensions given in Table I. Comparison between measurements and calculations (predicted) for the reflection coefficient are displayed in Fig. 6. As seen, the full-wave simulator and measured data agree quite well for both magnitude and phase of the reflection coefficient, thus validating the accuracy of the simulator. Also, note that for our FSS models, resistive cards [14] were used to suppress strong phase variations.

III. FSS Design Procedure

A simple circuit model to predict the electromagnetic behavior of a single-layer FSS plays a crucial role in the design process of multilayer FSS structures. Employing the full-wave simulator in an optimization loop is not necessarily a viable strategy in designing multilayer FSS structures since such an approach is time consuming and inefficient. On the other hand, once obtained, the circuit model can easily be incorporated into existing circuit optimizers to provide geometry parameters that satisfy a given objective.

In this section, we present an equivalent circuit model for a strip-dipole FSS. Our goal is to use this simple element as an example in understanding the FSS design for achieving nearly constant phase responses over a certain bandwidth. To this end, we first employ the equivalent circuit model to develop an initial design of the FSS. Full-wave simulation results are then carried out as a final step on the basis of the derived circuit parameters.

For a single-layer dipole FSS, the resonant behavior of the reflection coefficient suggests that a similar response can be obtained using an LC equivalent circuit. We use a first order transmission line/circuit (TL/CKT) model in conjunction with a simplex (direct search) curve-fitting algorithm [15] to determine the equivalent circuit parameters. The block diagram of this procedure is depicted in Fig. 7. As shown, a dipole FSS structure is first analyzed using the full-wave simulator, and the reflection coefficient (Γ) of the FSS is then utilized in the simplex search algorithm to determine the corresponding

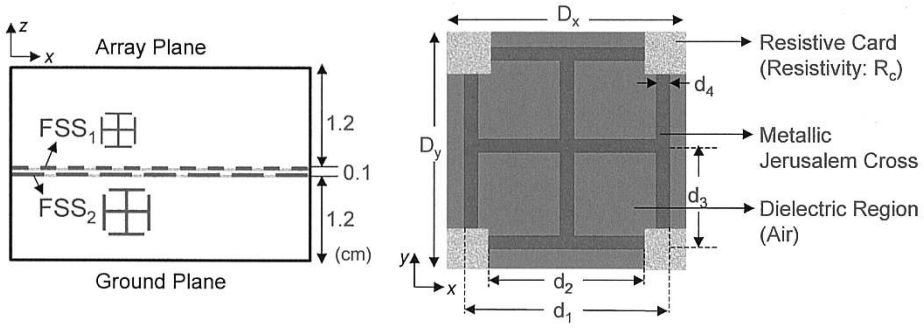

Fig. 5. Configuration and unit-cell geometry of the double-layer Jerusalem cross FSS.

TABLE I
DIMENSIONS OF THE STRUCTURE IN Fig. 5

(cm)	FSS_1	FSS_2
d_1	9.60	13.21
d_2	6.98	10.16
d_3	5.05	6.86
d_4	0.51	0.51
$D_{x(y)}$	10.67	13.72
$R_c(\Omega/cm^2)$	370	230

circuit parameters. In the design process, it is essential to relate the circuit parameters L and C to the geometrical parameters of the structure. For this purpose, various dipole geometries were simulated by varying their lengths (d) and widths (w) using the full-wave simulator. As a result of this study, the following design formulae were developed:

$$L = \frac{A_L}{d\sqrt{w}} Z_0 \text{ (nH)} \quad \text{and} \quad C = A_C\, d^3\sqrt{w}/Z_0 \text{ (nF)} \quad (1)$$

where the dipole dimensions d and w are in cm and $Z_0 = 377\,\Omega$. Also, A_L and A_C are some constants to be determined during the curve-fitting process. They are dependent on the dielectric constant and thickness of the substrate (ε_r, t), element separation (D_x, D_y), and incidence angle (θ_i, ϕ_i). For the specific case of a free-standing dipole FSS having unit cell dimensions $D_x = D_y = 7.5$ cm and normal incidence

$$A_L = 0.7674\ (\text{nsec} \cdot cm^{3/2} \cdot rad^{-1}) \quad \text{and}$$
$$A_C = 0.1811 \times 10^{-3} (\text{nsec} \cdot cm^{-7/2} \cdot rad^{-1}).$$

As an example, we display the reflection coefficient of a free-standing dipole FSS ($d = 5$ cm, $w = 0.625$ cm) along with its equivalent circuit ($L = 73.19$ nH, $C = 47.47$ fF) in Fig. 8. As seen, the reflection coefficient corresponding to the circuit model agrees sufficiently well with the actual reflection coefficient over a wide frequency band.

Note that the relations given in (1) represent a first-order TL/CKT model, valid only for a single-layer dipole FSS structure. Coupling between elements on the same FSS layer should be incorporated in the modeling to obtain a broad-band equivalent circuit representation, thus allowing periodicity parameters

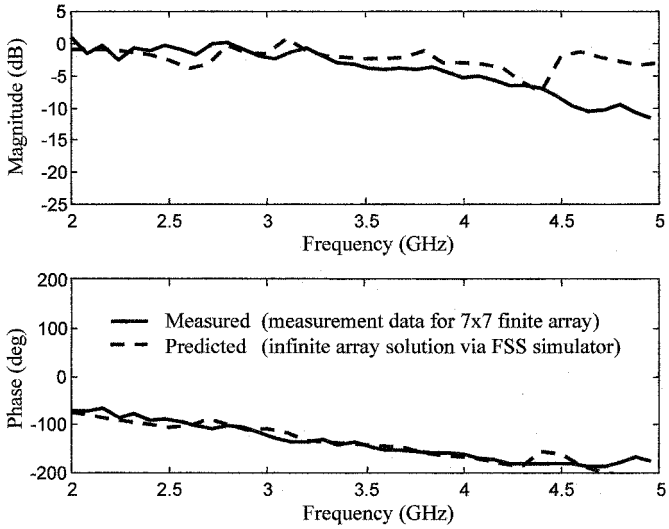

Fig. 6. Reflection coefficient of the double-layer Jerusalem cross FSS: comparison between predicted and measured data.

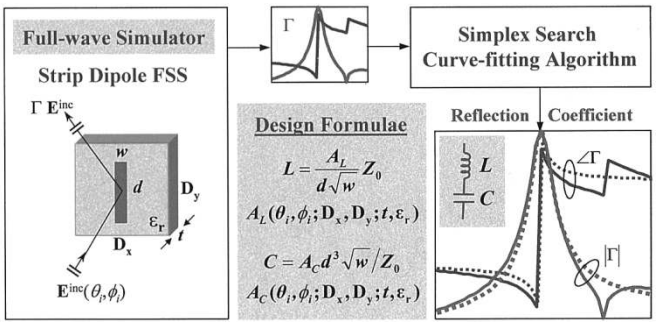

Fig. 7. Building the equivalent circuit model for a single-layer dipole FSS.

to be accounted for in the model. In addition, for different incidence angles, A_L and A_C must be re-evaluated.

This prototype circuit model can be used to design multilayer FSS structures. The FSS behavior can be approximated using stacks of equivalent LC circuits cascaded by inserting TLs between them. As an example, we consider the optimum design of a three-layer lossless dipole FSS configuration with the pass-band response in the frequency range of 1.5–3.5 GHz. The lengths and widths of dipoles are varied as well as the separation between the layers during the optimization process. The comparative results for the TL/CKT model and the full-wave simulation are displayed in Fig. 9. As seen, the optimization

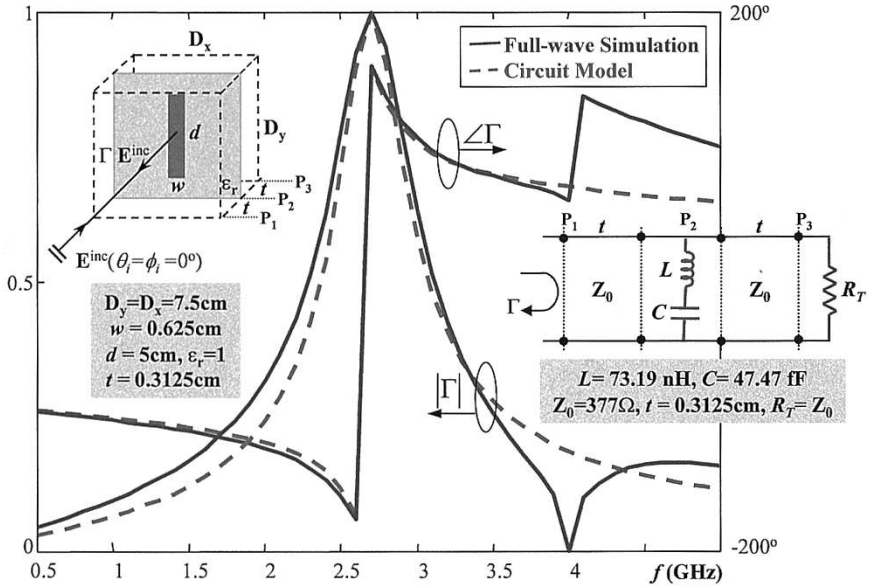

Fig. 8. Reflection coefficient of a free-standing dipole FSS: the full-wave simulation (solid) versus the circuit model (dashed).

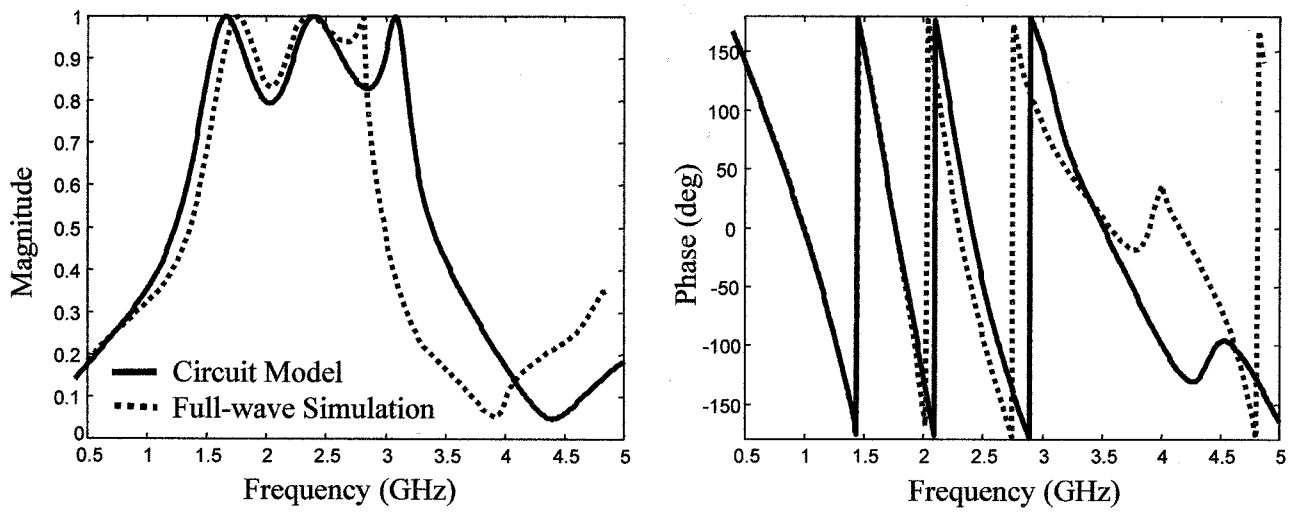

Fig. 9. Reflection coefficient of the three-layer dipole FSS structure: the circuit model (solid) versus the full-wave simulation (dashed).

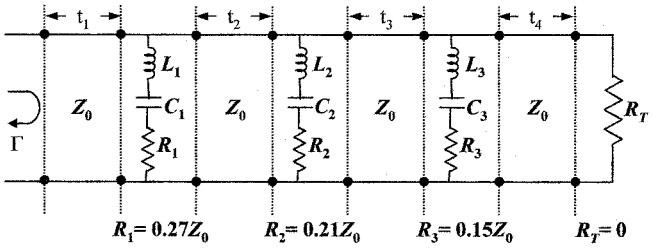

Fig. 10. Three-stage TL/CKT design to achieve the criteria given in (2).

based on the first order model agrees very well with the full-wave simulation in the frequency band of 0.5–2.5 GHz. However, the agreement deteriorates beyond 2.5 GHz since the first-order model design neglects higher-order mode coupling among the layers.

Of particular importance in assessing the results in Fig. 9 is that the phase of the reflection coefficient is highly oscillatory. Hence, with a lossless FSS structure, it is not possible to obtain a reflection coefficient having a nearly flat response. For a broad-band GP, sharp variations in the phase must be eliminated so that the reflected field from the FSS will have a nearly constant phase response. As such, this reflected field will add in congruence with the direct antenna-radiated field (Fig. 2). By analogy with circuit theory, the phase response can be smoothened out by introducing some loss in the FSS structure. Resistive cards (R-cards) can be placed on the FSS layers for this purpose to smoothen out the phase response in the pass-band at the expense of efficiency. The effect of R-cards can be included in the circuit model by adding a resistor in series with the LC branch of the equivalent circuit. As can be understood, there is a tradeoff between a flat-phase response and the amplitude of the reflection coefficient. Introducing R-cards in the structure allows for a smooth phase response, but decreases the reflection-coefficient amplitude.

Next, we consider such a multilayer FSS design incorporating R-cards to simulate a broad-band flat-phase GP.

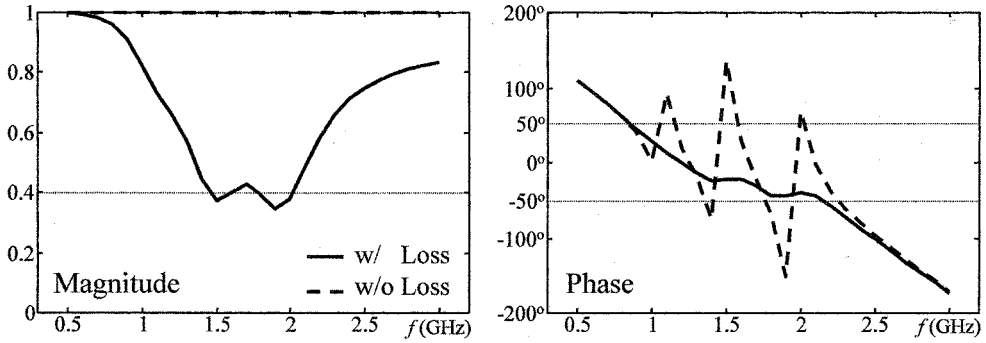

Fig. 11. Reflection coefficient of the three-stage TL/CKT design in Fig. 10 with and without loss.

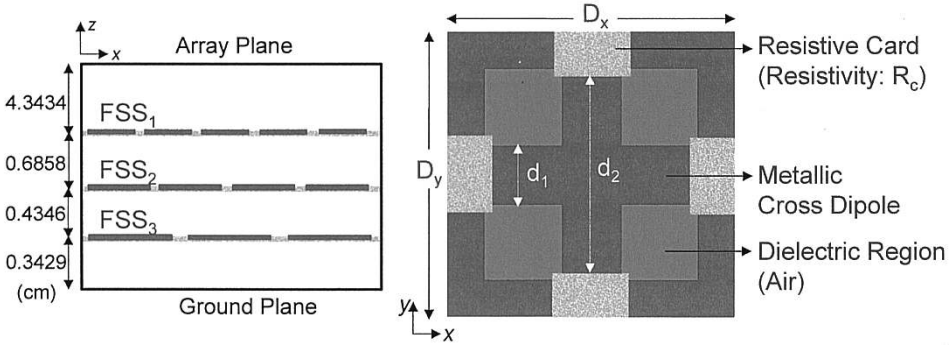

Fig. 12. Configuration and unit-cell geometry of the three-layer cross-dipole FSS.

A three-layer FSS structure has been designed to simulate a broad-band flat-phase GP for a practical reconfigurable array. In this case, the FSS is designed to reflect a wave that is in phase with the direct field radiated by the antenna toward the horizon (see Fig. 2). For practical purposes, the FSS design objectives for the reflection coefficient (Γ) are as follows:

$$\begin{aligned} &\text{Magnitude: } 0.4 < |\Gamma| < 1.0 \\ &\text{Phase: } -50^\circ < \angle\Gamma < 50^\circ \end{aligned} \tag{2}$$

These are based on achieving a maximum of 4-dB loss (direct + reflected; see Fig. 2) in reference to an ideal reflector with $\Gamma = 1\ell^{j0}$. First, according to the aforementioned criteria, a three-stage circuit modeling of the structure was devised as depicted in Fig. 10. To smoothen out the phase response, we introduced some loss by adding a resistor $(R_i, i = 1,2,3)$ in series with each LC branch of the circuit. Note that this structure is terminated by a short circuit, i.e., $R_T = 0$. In Fig. 11, the reflection coefficient of this three-stage TL/CKT design is shown for the cases with and without loss, i.e., $R_i > 0$ and $R_i = 0$ $(i = 1,2,3)$, respectively. As seen, the design objectives in (2) are achieved quite well in almost a 3:1 bandwidth by using the lossy TL/CKT design.

Next, based on the equivalent circuit model for a single-layer dipole FSS, the actual FSS structure was formed as shown in Fig. 12 with the dimensions given in Table II. As seen, this noncommensurate structure consists of closely-packed cross dipoles as FSS elements to achieve a broad-band and polarization-free response. The dimensions of strip dipoles forming a cross dipole on each FSS layer were determined by the equivalent model formulae (1). The structure is backed by a GP, representing the short circuit termination. In addition, the FSS elements are interleaved by R-cards to obtain the flat-phase response. In fact, these R-cards represent the resistors present in the TL/CKT design (see Fig. 10). The R-card parameters (resistivity and dimensions) were optimized to meet the design criteria (2). No design formula was used to relate the resistor values in the circuit model to the R-card parameters. However, the ratios of resistor values remained the same as those of the corresponding resistivity values, i.e., $R_1/R_3 = R_{c1}/R_{c3}$ and $R_2/R_3 = R_{c2}/R_{c3}$. In Fig. 13, the full-wave simulation results for the designed three-layer FSS structure are displayed for a normally incident plane wave. We observe that the design criteria for the reflection coefficient are indeed attained, whereas the resistive loading flattens the phase at the expense of some efficiency. Also, note that the circuit model response given in Fig. 11 agrees well with the actual response in Fig. 13. Though being a first-order model, the developed TL/CKT process has been very useful in understanding and designing of multilayer FSS structures.

TABLE II
DIMENSIONS OF THE STRUCTURE IN Fig. 12

(cm)	FSS_1	FSS_2	FSS_3
d_1	3.012	3.270	3.702
d_2	5.890	7.560	10.776
$D_{x(y)}$	10.0	12.0	16.0
$R_c(\Omega/cm^2)$	1800	1400	1000

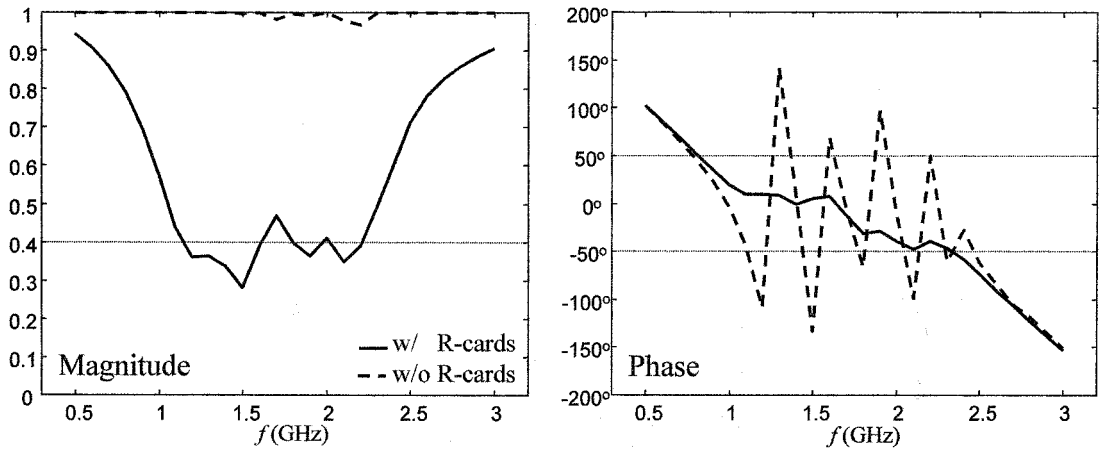

Fig. 13. Reflection coefficient of the three-layer FSS structure in Fig. 12 with and without resistive loading.

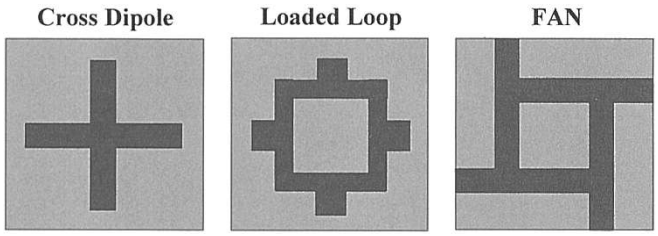

Fig. 14. FSS elements investigated as candidates for broad-band reflection.

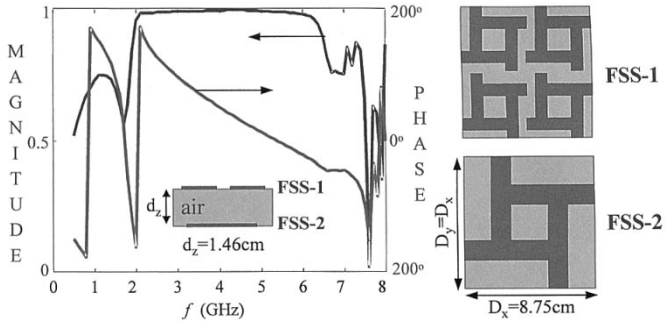

Fig. 15. Reflection coefficient of the two-layer FAN element FSS.

IV. FSS Element Design

To achieve broad-band operation for reconfigurable arrays, the emphasis must be on the phase control of the substrate reflection coefficient. Earlier, we demonstrated that a three-layer dipole FSS can achieve a fairly flat phase response from about 0.8 to 2.3 GHz. Of interest in this section is to minimize the FSS thickness (possibly using a single FSS layer) and to further ensure that the phase response is maintained at $|\text{phase}(\Gamma)| < 50°$. The choice of FSS elements plays a crucial role since these elements must also be broad-band to minimize the thickness of the FSS. Toward achieving this goal, various shapes of printed FSS elements were investigated using the full-wave simulator (some are shown in Fig. 14). We examined relations between element parameters and FSS response and considered coupling effects. It was found that bandwidth is enhanced when the FSS elements are brought close to each other within the same FSS layer. In addition, as expected, loaded elements yield broader bandwidths. Also, one could compromise between the individual FSS bandwidth and number of FSS layers included in the design. The displayed FAN[1] element in Fig. 14 was found quite attractive in terms of magnitude bandwidth and phase response. This FAN element can be thought of as a loaded loop. By tuning the lengths of the loads and the inner radius of the loop, we can control the resonance behavior of the FSS.

Once the FSS element is chosen, the desired response can then be synthesized by increasing the number of FSS layers and varying their separation. In particular, two layers of the FAN element FSS (see Fig. 14) provide broad-band reflection with unity amplitude over three octaves as seen in Fig. 15. Also, its phase response is not as oscillatory as that of the dipole. Because of this behavior, the FAN element is a preferred choice for a thin, broad-band FSS. Previously, it was also demonstrated that optimizing the resistive loading provides improved FSS phase performance. Relatively flat-phase ($\pm 50°$) can be achieved by reducing the reflected power (a loss of 3 dB or so) for an acceptable operation. In light of these observations, we designed a single-layer, resistive FAN element FSS to achieve the design criteria for the reflection coefficient. The configuration and unit-cell geometry of this novel FSS along with its response are shown in Fig. 16. As seen, a relatively flat-phase response is obtained over the whole band using only one layer of the resistive FAN element FSS. Next, we consider the reconfigurable printed antenna performance where the FSS is used as the GP.

[1]The common word "FAN" is used to denote the new FSS shape.

V. Reconfigurable Array Performance

Here we consider the performance of a reconfigurable dipole array placed over the designed FAN element FSS. The dipole length is altered using switches to operate at a different band without a need for changing the FSS design, which serves as a broad-band substrate. Reconfiguration of dipoles is depicted in Fig. 17 and the frequency band of interest is 0.8–3.2 GHz. When the switch is on, the dipole length becomes $\lambda/2$ at 1.2 GHz (low-band operation). When the switch is set at the off-state (open), the dipole length reduces to $\lambda/2$ at 2.0 GHz, thus forming the high-band configuration. In this case, besides the excited dipole, the remaining unconnected sections of the dipole are kept in the analysis and act as parasitic elements.

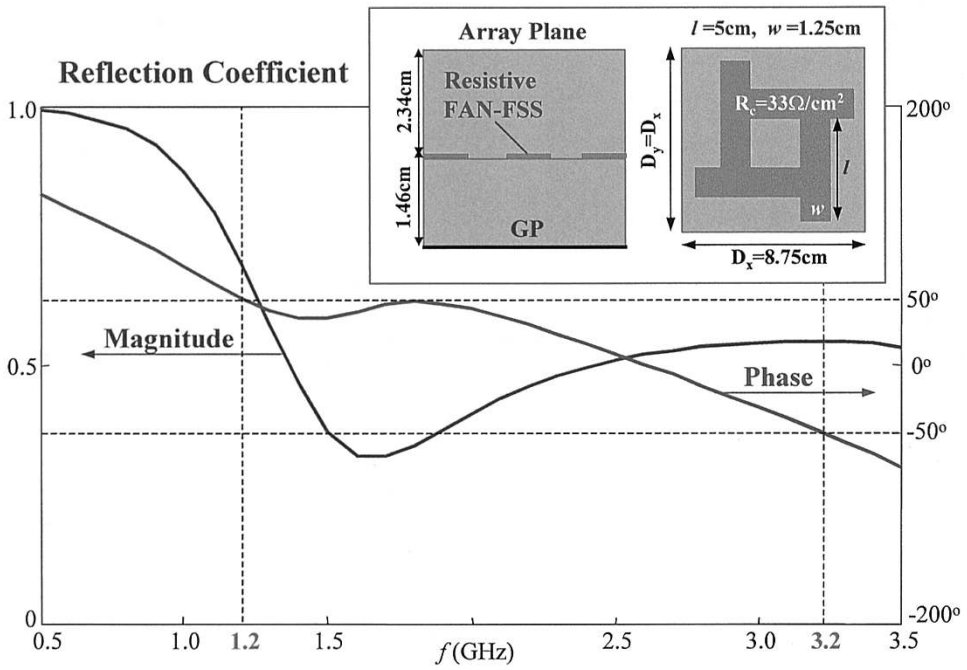

Fig. 16. Reflection coefficient of the resistive FAN element FSS.

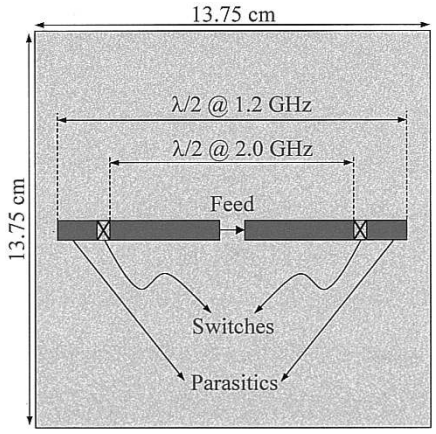

Fig. 17. Unit-cell geometry of the reconfigurable dipole array.

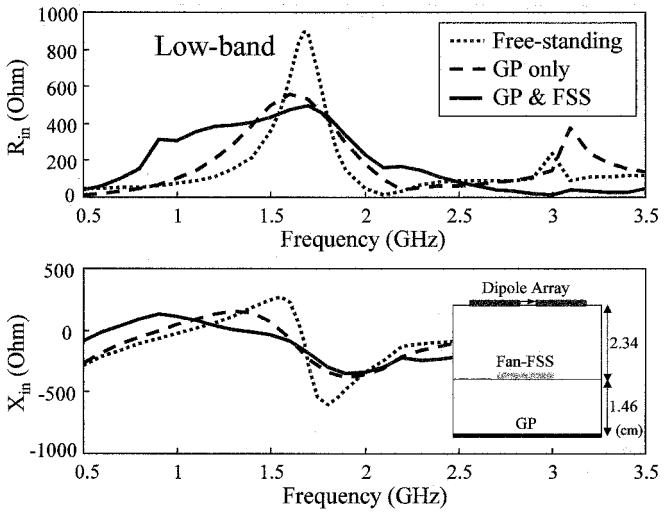

Fig. 18. Broadside scanning input impedance ($Z_{\rm in} = R_{\rm in} + jX_{\rm in}$) of the low-band dipole array for three cases: the free-standing array, the array backed by GP, and the array over the FAN-FSS and GP.

Note that the analysis results shown in this section were obtained by means of the full-wave simulator, whose accuracy for non-commensurate structures were validated previously (see Fig. 6).

We first demonstrate the improved bandwidth achieved for the dipole array in the presence of the FAN element FSS. In Fig. 18, we display the broadside scanning input impedance characteristics of the dipole array with and without the FSS for the low-band configuration. As seen, the bandwidth improvement with inclusion of the FSS is quite impressive when compared to free-standing dipoles as well as dipoles backed with a metallic GP only. This enhancement is due to the relatively flat-phase behavior of the FAN element FSS. Since the phase is maintained near 0°, the FSS serves to emulate a magnetic GP. As such, it can substantially enhance the radiation properties of the dipole array since the reflected field is in phase with that directly radiated by the antenna itself. In Fig. 19, we show the E plane radiation patterns at different frequencies. Note that these patterns were obtained by integrating the aperture currents over the unit cell. We observe that the FSS-GP provides significant improvement in radiation performance as compared to the purely metallic GP. Also, more than a 4-dB gain enhancement was achieved over the band by means of the FSS-GP as compared to the free-standing array configuration (despite the lossy FSS). At this point, one may ask whether the same performance could be achieved using a multilayered lossy dielectric above a GP instead. The multilayered lossy configuration will however lead to higher losses and to a much thicker ground plane.

For the high-band configuration, the switches (see Fig. 17) are now opened and the dipole length is shortened. Besides the fed-dipole, we now have parasitic strips present in the array plane, but these only cause a very slight shift in the frequency response. In Fig. 20, the input impedance characteristics of the

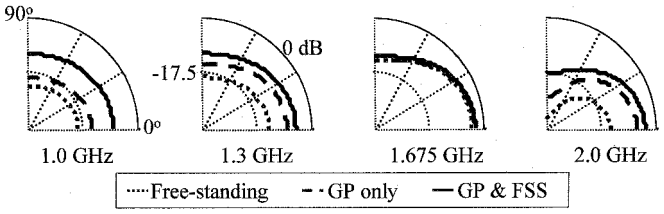

Fig. 19. E plane radiation patterns of the low-band dipole array at broadside (0° refers to broadside).

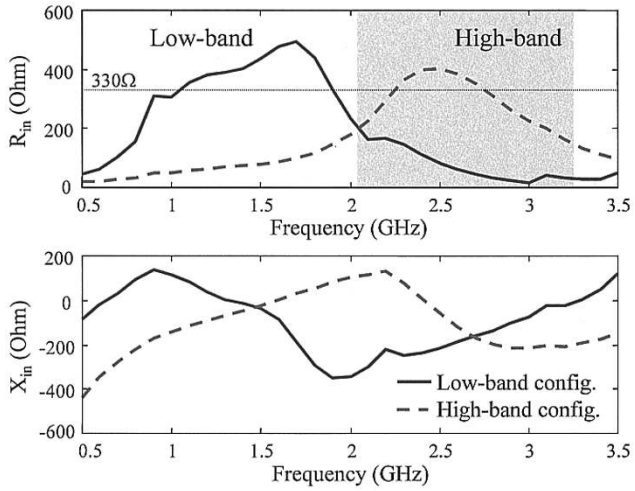

Fig. 20. Input impedance ($Z_{\text{in}} = R_{\text{in}} + jX_{\text{in}}$) of the reconfigurable dipole array over the resistively loaded FAN element FSS.

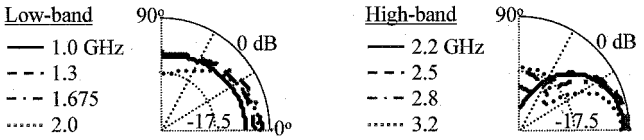

Fig. 21. E plane radiation patterns of the reconfigurable dipole array at broadside.

dipole array are displayed for the high-band configuration as well as the low-band. As seen, the reconfigurable dipole array over the resistively loaded FAN element FSS performs quite well over the entire 800 to 3200 MHz band. Note, however, that the location and dimensions of the FSS are kept the same (see Fig. 16) for both low and high band operations. In addition, in Fig. 21, the E plane radiation patterns for broadside scanning at different frequencies are displayed for the reconfigurable array, showing the broad-band radiation performance.

VI. Conclusion

In this paper, we presented FSS designs aimed at enhancing the performance of reconfigurable broad-band arrays when used as a ground plane (substrates) for such arrays. As an analysis and design tool, we used a fast full-wave simulator employing the hybrid FE-BI method in conjunction with the FSDA. The full-wave simulator is capable of dealing with noncommensurate periodicities, and the accuracy of the simulator was validated with the measured data for a double-layer Jerusalem cross FSS test-bed.

We demonstrated that if the reflection coefficient phase for the FSS is maintained near 0°, the FSS serves to emulate a magnetic GP. As such, it can substantially enhance the radiation properties of the dipole array since the reflected field adds in phase with that directly radiated by the array itself. To achieve this goal, we designed a novel FSS consisting of resistively loaded "FAN" elements. This FSS test-bed was shown to provide a relatively flat-phase reflection for at least one octave at the expense of some efficiency loss due to the resistive loading. The designed FSS was then used as a substrate to enhance the dipole array performance. It was demonstrated that the FSS allowed the operation of the reconfigurable array over a 3:1 bandwidth. The broadside impedance of the dipole was maintained nearly 330 Ω over this band.

References

[1] R. Coccioli, F.-R. Yang, K.-P. Ma, and T. Itoh, "Aperture-coupled patch antenna on UC-PBG substrate," *IEEE Trans. Microwave Theory Tech.*, vol. 47, pp. 2123–2130, Nov. 1999.

[2] J. D. Shumpert, W. J. Chappell, and L. P. B. Katehi, "Parallel-plate mode reduction in conductor-backed slots using electromagnetic band gap substrates," *IEEE Trans. Microwave Theory Tech.*, vol. 47, pp. 2099–2104, Nov. 1999.

[3] R. Mittra, C. H. Chan, and T. Cwik, "Techniques for analyzing frequency selective surfaces—A review," *Proc. IEEE*, vol. 76, pp. 1593–1615, Dec. 1988.

[4] B. A. Munk, *Frequency Selective Surfaces*. New York, NY: Wiley, 2000.

[5] S. Tibuleac, R. Magnusson, T. A. Maldonado, P. P. Young, and T. R. Holzheimer, "Dielectric frequency-selective structures incorporating waveguide gratings," *IEEE Trans. Antennas Propagat.*, vol. 48, pp. 553–561, Apr. 2000.

[6] H. Contopanagos, L. Zhang, and N. G. Alexopoulos, "Thin frequency-selective lattices integrated in novel compact MIC, MMIC, and PCA architectures," *IEEE Trans. Microwave Theory Tech.*, vol. 46, pp. 1936–1948, Nov. 1998.

[7] H. Aroudaki, V. Hansen, H.-P. Gemund, and E. Kreysa, "Analysis of low-pass filters consisting of multiple stacked FSSs of different periodicities with applications in the submillimeter astronomy," *IEEE Trans. Antennas Propagat.*, vol. 43, pp. 1486–1491, Dec. 1995.

[8] J. L. Volakis, T. Ozdemir, and J. Gong, "Hybrid finite-element methodologies for antennas and scattering," *IEEE Trans. Antennas Propagat.*, vol. 45, pp. 493–507, Mar. 1997.

[9] T. F. Eibert and J. L. Volakis, "Fast spectral domain algorithm for rapid solution of integral equations," *Electron. Lett.*, vol. 34, no. 13, pp. 1297–1299, June 1998.

[10] E. W. Lucas and T. W. Fontana, "A 3-D hybrid finite element/boundary element method for the unified radiation and scattering analysis of general infinite periodic arrays," *IEEE Trans. Antennas Propagat.*, vol. 43, pp. 145–153, Feb. 1995.

[11] D. T. McGrath and V. P. Pyati, "Periodic structure analysis using a hybrid finite element method," *Radio Sci.*, vol. 31, no. 5, pp. 1173–1179, Sept./Oct. 1996.

[12] T. F. Eibert, J. L. Volakis, D. R. Wilton, and D. R. Jackson, "Hybrid FE/BI modeling of 3D doubly periodic structures utilizing triangular prismatic elements and a MPIE formulation accelerated by the Ewald transformation," *IEEE Trans. Antennas Propagat.*, vol. 47, pp. 843–850, May 1999.

[13] A. K. Bhattacharyya, "Analysis of multilayer infinite periodic array structures with different periodicities and axes orientations," *IEEE Trans. Antennas Propagat.*, vol. 48, pp. 357–369, Mar. 2000.

[14] T. B. A. Senior and J. L. Volakis, "Sheet simulation of a thin dielectric layer," *Radio Sci.*, vol. 22, no. 7, pp. 1261–1272, Dec. 1987.

[15] J. A. Nelder and R. Mead, "A simplex method for function minimization," *Computer J.*, vol. 7, pp. 308–313, 1965.

Yunus E. Erdemli (S'96–M'02) was born on March 12, 1970 in Tatvan, Turkey. He received the B.S. degree in electrical engineering from Middle East Technical University, Ankara, Turkey, in 1992 and the M.S. and Ph.D. degrees from the University of Michigan, Ann Arbor, both in electrical engineering, in 1996 and 2002, respectively.

In 1992, he joined Turkish Military Electronics, Inc., Ankara, Turkey, as an RF Design Engineer. In 1993, he was awarded an Abroad Ph.D. Fellowship by The Higher Educational Council of Turkey. As part of this grant, he started his graduate studies at the University of Michigan in 1994, and he was sponsored by Kocaeli University, Izmit, Turkey, until 2000. During 1994–2002, he was a graduate Research Assistant at the University of Michigan Radiation Laboratory, Ann Arbor, where he also served as a Postdoctoral Research Associate. Currently, he is an Assistant Professor in the Department of Electronics and Computer Education, Kocaeli University, Ismit, Turkey. His research interests include numerical analysis and design of conformal/reconfigurable arrays and frequency selective surfaces/volumes for broad-band applications, and model order reduction algorithms for electromagnetics.

Kubilay Sertel was born on June 27, 1973, in Tekirdag, Turkey. He received the B.S. degree from the Middle East Technical University, Ankara, Turkey, the M.S. degree from Bilkent University, Ankara, Turkey, and the Ph.D. degree from the University of Michigan, Ann Arbor, all in electrical engineering, in 1995, 1997, and 2003, respectively.

He is currently a Research Associate with the ElectroScience Laboratory, The Ohio State University, Columbus. Prior to this position, he worked as a graduate Research Assistant, University of Michigan, Ann Arbor, and at Bilkent University, Ankara, Turkey. His research areas include electromagnetic theory, computational electromagnetics, integral equation and hybrid methods, fast and efficient methods for large-scale electromagnetics problems, and parallel implementations of fast algorithms.

Roland A. Gilbert (S'74–M'86) received the M.S.E.E. and Ph.D. degrees from the University of Illinois, Urbana, and the B.S.E.E. degree from the University of Maine, Orono.

He has been with BAE Systems, Nashua, NH, since 1985 where he is currently an Engineering Fellow. His research is in the development of broad-band, structurally integrated multifunction optically reconfigurable antenna arrays. This research interest has also included antenna scattering and the development of CEM tools for conformal, quasi-periodic scattering structures. His current work is in the development of highly efficient, electrically small radiators and the development of methodologies to determine coupling between antenna arrays in the presence of large complex scatterers. Before joining BAE Systems, he was with the U.S. Army Corps of Engineers, Champaign, Il.

Dr. Gilbert is a Member of Antennas and Propagation Society of the IEEE.

Daniel E. Wright received the B.S.E.E. degree in communications and the M.S.E.E. degree in electromagnetics from Michigan Technological University, Houghton, in 1988 and 1990, respectively.

He has been with BAE Systems, Nashua, NH, since 1999, where he is currently a Principal Electrical Engineer in the Advanced Technology Division. From 1992 to 1997, he was with Lockheed Martin, Nashua, NH, working on low-observables signature technology and antenna/array design, analysis, test, and fielding. At Lockheed Martin, he also served as a Principal Investigator for developmental engineering activities focused on microwave systems and antenna/array technology development. His current interests are in wideband, reconfigurable, and low-observable apertures for platform integration, numerical modeling techniques, and component fabrication and testing. He has also worked on multifunction EW arrays and CNI apertures and EW and CNI aperture suites.

John L. Volakis (S'77–M'82–SM'89–F96) was born on May 13, 1956, in Chios, Greece. He received the B.E. degree (summa cum laude) from Youngstown State University, Youngstown, OH, in 1978, and the M.Sc. and Ph.D. degrees from The Ohio State University (OSU), Columbus, in 1979 and 1982, respectively.

From 1982 to 1984, he was with Rockwell International, Aircraft Division, and from 1978 to 1982, he was a Graduate Research Associate at the OSU ElectroScience Laboratory. He has been a Professor in the Department of Electrical Engineering and Computer Science, University of Michigan, Ann Arbor, since 1984. He also served as the Director of the Radiation Laboratory from 1998 to 2000. Since January 2003, he has been the Roy and Lois Chope Chair Professor of Engineering at The Ohio State University and also serves as the Director of the ElectroScience Laboratory. His primary research deals with the development and application of computational and design techniques to scattering, antennas, and bioelectromagnetics. He has published 175 articles in major refereed journal articles, more than 190 conference papers, 17 book chapters, and coauthored two books: *Approximate Boundary Conditions in Electromagnetics* (IEEE Press: Piscataway, NJ, 1995) and *Finite Element Method for Electromagnetics* (IEEE Press: Piscataway, NJ, 1998). He was an Associate Editor of *Radio Science* from 1994 to 1997. He is now an Associate Editor for the *J. Electromagnetic Waves and Applications*

Dr. Volakis received the University of Michigan College of Engineering Research Excellence Award in 1998, and in 2001, he received the Department of Electrical Engineering and Computer Science Service Excellence Award. He served as an Associate Editor of IEEE TRANSACTIONS ON ANTENNAS AND PROPAGATION from 1988 to 1992. He chaired the 1993 IEEE Antennas and Propagation Society Symposium and Radio Science Meeting, and was a member of the AdCom for the IEEE Antennas and Propagation Society from 1995 to 1998. and the *IEEE Antennas and Propagation Society Magazine*. He is a member of Sigma Xi, Tau Beta Pi, Phi Kappa Phi, and Commission B of URSI. He is also listed in several "Who's Who" directories, including *Who's Who in America*.